Drops ejection from a capillary nozzle by Drop-On-Demand technology

Sanda-Carmen Georgescu, Edouard Canot, Jean-Luc Achard, Arthur Soucemarianadin

DROPS EJECTION FROM A CAPILLARY NOZZLE BY DROP-ON-DEMAND TECHNOLOGY

Sanda-Carmen GEORGESCU[1], Édouard CANOT[2], Jean-Luc ACHARD[3], Arthur SOUCEMARIANADIN[4]

[1] Corresponding Author. Hydraulics Department, University "Politehnica" of Bucharest. 313 Spl. Independentei, S6, RO-060042, Bucharest, Romania. Tel.: +40 723624418, Fax: +40 214029865, E-mail: carmen@hydrop.pub.ro
[2] Institut de Recherche en Informatique et Systèmes Aléatoires, INRIA, Rennes, France. E-mail: Edouard.Canot@irisa.fr
[3] Laboratoire des Écoulements Géophysiques et Industriels (LEGI), Grenoble, France. E-mail: Jean-Luc.Achard@hmg.inpg.fr
[4] Laboratoire des Écoulements Géophysiques et Industriels (LEGI), Grenoble, France. E-mail: Arthur.Soucemarianadin@ujf-grenoble.fr

ABSTRACT

Drop-on-Demand (DOD) technology enables to control the ejection of drops, from a vertically capillary nozzle, by piezoelectric stimulation. DOD applies in microfluidics, from the ink-jet printers to Bio-MEMS. This study emphasizes on the numerical simulation of the drop evolution during its formation and ejection by DOD technology. The highly distorted interface evolution represents an axisymmetric transient free-boundary problem, which is modelled here through a Boundary Element Method. An irrotational flow model can reproduce most observed experimental data on drop size, velocity, frequency, and conditions for non-satellite formation. Viscous effects are included to some extent, as it is allowed for potential flows of fluids with constant viscosity, the normal viscous stress at the interface being expressed in terms of the velocity potential. The time progression is made with a 4th order Runge-Kutta explicit numerical scheme. The time step is varied upon a stability criterion. The interface evolution is determined through a Lagrangian description of a variable number of nodes, unevenly redistributed on the boundary at each time step. The numerical code accuracy is evaluated through the global mechanical energy balance, expressed only in surface integrals terms. Our computed results fit well the available DOD data for ejected drops with volume of picolitres order.

Keywords: Boundary Element Method, drop formation, Drop-on-Demand, ink-jet fluid microdispensing, interface distortion

NOMENCLATURE

Fr	[-]	Froude number
H	[$1/m$]	total curvature
M		observation point
P		singularity point
R	[m]	orifice radius; length scale
R_1, R_2	[m]	local principal radii of curvature
Re	[-]	Reynolds number
We	[-]	Weber number
dA	[m^2]	axisymmetric surface element
g	[m/s^2]	gravity
n	[m]	normal co-ordinate
r	[m]	radial co-ordinate
s	[m]	curvilinear abscissa
t	[s]	time
v	[m/s]	velocity
z	[m]	axial co-ordinate
Δs	[m]	arc length
Δt	[s]	time step
Ω		domain in a meridian plane
Σ		surface; interface
β	[rad]	azimuthal angle
ϕ	[m^2/s]	velocity potential
μ	[$Pa \cdot s$]	dynamic viscosity of the liquid
ρ	[kg/m^3]	density of the liquid
σ	[N/m]	surface tension

Subscripts and Superscripts

D	domain
L	liquid
P	related to the singularity point
W	solid wall
n	normal direction
z	axial direction
*	dimensionless variable

1. INTRODUCTION

There are two main approaches in ink-jet printing technology [1].

Within the "Continuous, Charge and Deflect" ink-jet printing technology, also called CIJ for Continuous Ink-Jet, the fluid under pressure issues from an orifice and breaks up into uniform drops by

the amplification of capillary waves induced onto the jet, usually by an electromechanical device. The ejected drops are electrically charged and deflected to their desired location. This approach is suitable for high-speed coverage of relatively large areas. The "Continuous, Charge and Deflect" ink-jet printing technology has been studied for the past 30 years: the characteristics of the ejected drops, as well as the conditions for satellite droplets formation are well known and analysed in [2-5].

Within the now more widely used "Drop-on-Demand" (DOD) ink-jet printing technology, smaller drops can be ejected from the device orifice, by applying a stimulation method (piezoelectric, or thermal). A DOD device produces drops of 20-100 microns in diameter, which are approximately equal to the diameter of the drop generator orifice. The DOD technology enables to control the size, velocity and frequency of the ejected drops. The piezoelectric DOD ink-jet method is commonly used, and the present paper will focus on it, i.e. on the drop ejected at a capillary nozzle tip, when a voltage pulse is applied to the nozzle-transducer, which is placed up-stream of the nozzle on the capillary. Piezoelectric ink-jet print heads have dominated the DOD industrial and commercial market for last two decades, because they offer high jetting frequency, long life expectancy, and the ability to jet a wide range of fluids under harsh working conditions [6]. The piezoelectrically driven DOD ink-jet printing technology has been studied experimentally [7-9] and/or numerically [10-12], in order to depict the ejected drops characteristics, and the conditions for non-satellite formation. The drop behaviour depends on the velocity profile at the orifice level, thus on the nozzle-transducer [6, 9, and 13]. The characteristics of the ejected drops are also influenced by the fluid properties [14, 15].

The DOD study is sustained by its many applications in microfluidics, ranging from the classical ink-jet printers, to various microdispensers and nanolitre dispensers [16-18] in chemical and pharmaceutical engineering, to jet printing for large area electronics [19, 20], as well as to DNA chips (the deposition of polymeric fluids on microchips for DNA in-situ synthesis) [21].

The present paper points on the numerical simulation of drop evolution during its formation at a vertical capillary tip, and its ejection by piezoelectrically driven DOD technology. The phenomenon involves strong nonlinear and coupled effects. The rapidity of the phenomenon, of microseconds order, and the space scales, of microns order, induce difficulties in experimental investigations. The advantage of numerical computations consists in analysing a large spectrum of droplet sizes, velocities, frequencies, and conditions for non-satellite formation. The modelling is achieved through an axisymmetric Boundary Element Method (BEM), assuming an irrotational flow of a viscous fluid [22], by using a personal numerical code built in Fortran. The numerical code has been validated in ultra-high speed interface hydrodynamics, especially to simulate the collapsing interface evolution for bursting bubbles at a free surface, finalised by microjet breaking and droplets ejection [23, 24].

Initial conditions, boundary conditions, and governing motion equations for the physical model are depicted in the second section of the present paper. The numerical procedure is outlined in the 3rd section. Results and comments are presented in the 4th section.

2. PROBLEM STATEMENT

An axisymmetric liquid domain Ω_L is considered in a meridian plane rOz (Figure 1). Inside the capillary nozzle, the domain is bounded by the liquid surface Σ_L in a radial direction. Laterally, it is bounded by the vertical solid wall Σ_W of the cylindrical nozzle, and at its bottom by the gas-liquid interface (drop surface) Σ, which is attached at the nozzle orifice edge. The orifice level is set at $z = 0$.

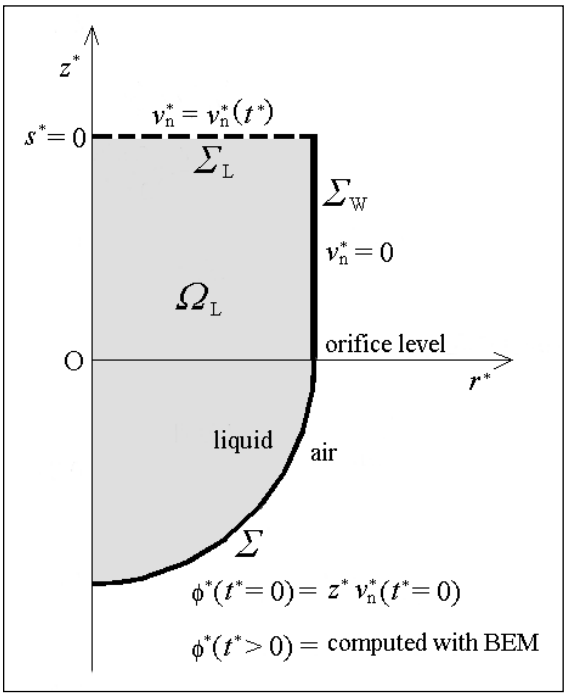

Figure 1. Geometrical configuration and boundary conditions

An outward normal unit vector is considered on the domain boundary. On the Oz axis, at the liquid surface Σ_L level, the curvilinear abscissa s is set to zero; its value increases when moving to the right along Σ_L, then downward along the wall Σ_W, then along the drop surface Σ, and reaches its maximum at the drop apex, on the Oz axis. Between the

tangential unit vector at any point on the boundary, and the radial unit vector, the azimuthal angle is denoted as β.

The orifice radius R is adopted as length scale, σ/R as pressure scale, $\sqrt{\sigma/(R\rho)}$ as velocity scale, where σ is the surface tension and ρ is the liquid density. The ratio between the length and velocity scale gives the time scale. Accordingly, the Weber number equals the unity, $We=1$, the Froude number is $Fr=\sigma/\left(\rho g R^2\right)$, and the Reynolds number is $Re=\sqrt{\rho\sigma R}/\mu$, where μ is the dynamic viscosity of the liquid. Dimensionless variables will be denoted with an asterisk. At the free drop surface, the adjacent gas pressure is assumed to be constant, since the gas inertia is neglected.

A potential liquid flow assumption is appropriate because of the impulsive character of the phenomenon. The dimensionless equations governing the potential liquid flow are classically the Laplace equation $\nabla^2\phi^*=0$ for the velocity potential ϕ^*, and the Euler's equation. The velocity v is defined by its normal component $\partial\phi^*/\partial n^*$, and tangential component $\partial\phi^*/\partial s^*$. In this type of model, viscous effects can be partially considered through a boundary condition, namely the normal momentum balance at any point of the interface Σ, which includes the normal viscous stress at the interface: $2\mu\left(\partial v_{\mathrm{n}}/\partial n\right)$, where v_{n} is the normal component of the velocity.

Combining the Laplace equation and the Euler's equation in order to reduce the pressure terms, yields the dimensionless Bernoulli's equation, i.e. the local time derivative of the velocity potential:

$$\frac{\partial\phi^*}{\partial t^*}=-\frac{\left(v^*\right)^2}{2}-\frac{H^*}{We}-\frac{z^*}{Fr}-\frac{2}{Re}\frac{\partial^2\phi^*}{\partial n^{*2}}. \qquad (1)$$

The dimensionless total curvature is written $H^*=\left(1/R_1^*+1/R_2^*\right)$, where R_1^* and R_2^* are the corresponding dimensionless local principal radii of curvature. There are distinct forms of Eq. (1) on the axis of symmetry Oz, and outside. The singularities at $r^*=0$ are removed by taking into account that on the Oz axis, the axisymmetric curvature, $1/R_2^*=\left(\sin\beta\right)/r^*$, equals the planar curvature, $1/R_1^*=\partial\beta/\partial s^*$. The expressions of the normal second derivative of the velocity potential $\partial^2\phi^*/\partial n^{*2}$ outside of the symmetry axis Oz, and on that axis, are defined in [23, 25].

Initial and boundary conditions are functions of the stimulation process, i.e. they depend on the excitation waves that are converted into velocity variations at the capillary nozzle tip. The hydrodynamics of the viscous liquid inside the capillary nozzle has been obtained by solving the Navier-Stokes equation [9, 26]: the imposed periodical wall deformation produces perturbations of the pressure field inside the capillary, and subsequently perturbations of the velocity field. So, the velocity reaches a peak during the voltage pulse, and relaxes after. For example [9], over a period of 0.1 *ms*, and voltage pulse duration of 20 μ*s*, the maximum axial velocity inside the capillary nozzle varies between about 3.2 *m/s* (at a voltage of 50 *V*) and 6.5 *m/s* (at 100 *V*).

Firstly, the resulting time dependent axial velocity profile inside the capillary nozzle (parabolic Poiseuille profile), has been averaged to obtain the mean axial velocity profile [26], for a voltage of 80 *V*. Secondly, its averaged form has been approximated for the BEM computations. The dimensionless time dependent normal velocity profiles $v_{\mathrm{n}}^*=v_{\mathrm{n}}^*\left(t^*\right)$ from Figure 2 are considered for BEM computations within this paper. The upper frame of Fig.2 corresponds to distilled water: at the initial moment, and over the first 8.5% of each period between two consecutive voltage pulses, the normal velocity value is set to $v_{\mathrm{n}}^*\left(t^*\right)=2$. The lower frame of Fig.2 corresponds to ink: at $t^*=0$, and over the first 9.9% of each period (of 3.42 dimensionless duration) between two consecutive voltage pulses, the normal velocity is $v_{\mathrm{n}}^*\left(t^*\right)=2.5$. In both frames, drop ejection instants are marked (by triangles). Ink drop ejection requests a higher maximum v_{n}^* value inside the capillary (so, a higher voltage), and a shorter period (ink being 8.7 times more viscous than water).

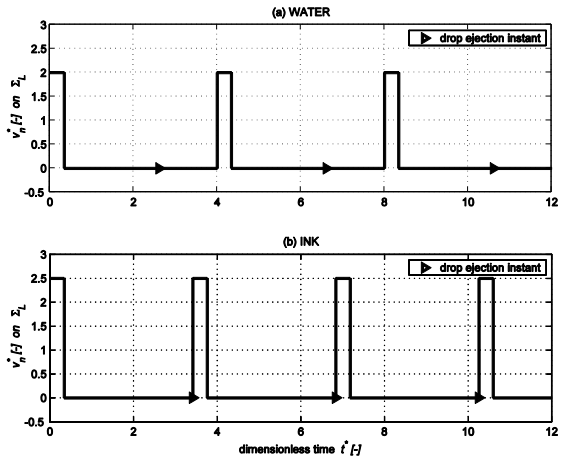

Figure 2. Dimensionless profile of the time dependent normal velocity inside the capillary nozzle, for water (a) and ink (b), used in BEM

For the BEM computations, the normal velocity profile $v_{\mathrm{n}}^*=v_{\mathrm{n}}^*\left(t^*\right)$ inside the capillary nozzle (Fig. 2) is inserted as a Neumann type boundary condition on the liquid surface Σ_{L} (Fig. 1). A

Neumann type boundary condition also corresponds to the solid wall Σ_W, where the normal velocity is zero. At the initial moment, the boundary conditions of Dirichlet type on the interface Σ are: $\phi^*(t^*=0)=z^* v_n^*(t^*=0)$. For further moments, the velocity potential $\phi^*(t^*>0)$ on Σ is obtained within the BEM (Fig. 1).

In the absence of non-linear analytical tests, the evaluation of numerical code accuracy is checked through the global mechanical energy balance, expressed only in surface integrals terms [23]:

$$\frac{d}{dt^*}\left(\frac{1}{2}\int_{\Sigma_D}\phi^*\frac{\partial\phi^*}{\partial n^*}dA^*+\frac{1}{We}\int_{\Sigma}dA^*\right)+$$
$$+\frac{d}{dt^*}\left(\frac{1}{2Fr}\int_{\Sigma}(z^*)^2 dA^*\right)= \qquad (2)$$
$$=-\frac{2}{Re}\int_{\Sigma_D}\frac{\partial\phi^*}{\partial n^*}\frac{\partial^2\phi^*}{\partial n^{*2}}dA^*,$$

where $\Sigma_D=\Sigma_L\cup\Sigma_W\cup\Sigma$ is the liquid domain boundary; dA^* is the dimensionless axisymmetric surface element. The dissipation of the mechanical energy due to shear viscosity depends only on the normal component of the velocity, and on the normal second derivative of the velocity potential, $\partial^2\phi^*/\partial n^{*2}$. Upon azimuthal integration, the mechanical energy balance deals with line integrals of the terms computed through the BEM, thus being easy to implement in the computational procedure.

3. NUMERICAL METHOD

The Boundary Element Method has been used in modelling the drop formation of the continuous jet [3], or the jet atomization [29], but under simpler assumptions, like the pure potential fluid flow, and even the absence of the gravity in [29]. Within the present study, the DOD modelling is achieved through a BEM, by assuming a potential flow of a viscous fluid [22]; it is a new approach for this type of process, and first results are presented in [26].

The drop surface Σ, highly distorted during its formation, represents a transient free-boundary problem that involves two types of calculations. We have indeed to cope with the task of calculating the potentials at a sequence of instants $t^*\in\{\Delta t^*,2\Delta t^*,\ldots$ $\ldots,(k-1)\Delta t^*,\ldots\}$. The small time step Δt^* is selected according to rules further defined. Firstly, a time-stepping scheme applied to Eq. (1) allows to link known values of the position of fluid particles on the interface, and of the velocity potential values on the same interface, evaluated at $t^*=(k-1)\Delta t^*$, to the corresponding values of these quantities at the following instant $t^*=k\,\Delta t^*$. Then, the potential values being known from this first type of calculation on the interface Σ, and the normal velocity components being also known on $\Sigma_L\cup\Sigma_W$ at $t^*=k\,\Delta t^*$, the Laplace equation can be solved with the BEM, to obtain the velocity potential values at the same instant $t^*=k\,\Delta t^*$ in the whole liquid domain. The time stepping technique requiring the normal component $\partial\phi^*/\partial n^*$, and tangential component $\partial\phi^*/\partial s^*$ of the velocity [27] on the interface Σ, can then be used again to connect the instants $t^*=k\,\Delta t^*$ and $t^*=(k+1)\Delta t^*$.

Within the second type of calculation, the Boundary Element Method allows replacing the Laplace's equation extended in the whole liquid domain Ω_L, by a second kind Fredholm integral equation extended only on the domain boundary Σ_D. For this direct BEM computation, the velocity field is generated by source and normal doublet type singularities spread over Σ_D. The integral equation on Σ_D is written:

$$-\int_{\Sigma_D}\phi^*(P)\frac{\partial\left(1/|MP|^*\right)}{\partial n_P^*}dA_P^*+$$
$$+\int_{\Sigma_D}\left(1/|MP|^*\right)\frac{\partial\phi^*(P)}{\partial n_P^*}dA_P^*=2\pi\,\phi^*(M), \qquad (3)$$

where $|MP|^*$ is the dimensionless distance between the observation point $M\in\Sigma_D$ and the singularity point P. The kinetic conditions of Neumann type on the surfaces Σ_L and Σ_W, where the normal velocity is known, as well as of Dirichlet type on the interface Σ, where the velocity potential is known, have been already depicted in the previous section (Fig.1).

The temporal interface evolution, which is based on Eq. (1), allows a Lagrangian description of a variable number of nodes $M(r^*(t^*),z^*(t^*))$, representing the position of fluid particles, unevenly redistributed on the boundary $\Sigma_D(t^*)$ at each instant, with respect to some criteria like the adaptation at the surface gradients [23]. This leads to a concentration of nodes at places where the interface's curvature is important, or where two portions of the interface approach one another. Thus, the simulation of the interface evolution is performed during the whole process, without applying any smoothing techniques that can affect the physics of the phenomenon.

The time step Δt^* is varied in accordance with a stability criterion, linked to the gravity-capillary dispersion equation [28]:

$$\Delta t^*\le 2\left(\frac{\pi^3}{We\left(\Delta s_{min}^*\right)^3}+\frac{\pi}{Fr\,\Delta s_{min}^*}\right)^{-0.5}, \qquad (4)$$

where $\Delta s^*_{\min}$ is the minimum value of the arc length measured between two consecutive points of the boundary $\Sigma_D(t^*)$.

The time progression is made with an explicit numerical scheme of 4th order Runge-Kutta type. Within this scheme, the material derivative of the velocity potential is defined by:

$$\frac{D\phi^*}{Dt^*} = (v^*)^2 + \left.\frac{\partial \phi^*}{\partial t^*}\right|_{\text{Eq.(1)}} . \tag{5}$$

The derivatives of the polar co-ordinates are:

$$\begin{aligned} \frac{Dr^*}{Dt^*} &= -\frac{\partial \phi^*}{\partial n^*}\sin\beta + \frac{\partial \phi^*}{\partial s^*}\cos\beta , \\ \frac{Dz^*}{Dt^*} &= \frac{\partial \phi^*}{\partial n^*}\cos\beta + \frac{\partial \phi^*}{\partial s^*}\sin\beta . \end{aligned} \tag{6}$$

4. RESULTS AND COMMENTS

The numerical modelling of drop evolution during its formation at a vertical capillary tip, and its ejection by piezoelectrically driven DOD technology has been systematically performed for distilled water and ink (at $20^{\circ}C$), for different orifice sizes, $R \in [13;100]\mu m$, in order to compare numerical and experimental data. Ink's physical properties [9, 26] are: $\rho = 1019\, kg/m^3$, $\mu = 8.7 \cdot 10^{-3}\, Pa \cdot s$, and $\sigma = 0.034\, N/m$. According to the investigated orifice sizes, the Froude and Reynolds numbers vary between the limits $Fr \in [743; 43954]$, $Re \in [30.6; 85]$ for distilled water, and $Fr \in [340; 20125]$, $Re \in [2.44; 6.76]$ for ink. The Weber number equals always the unity, $We = 1$, because of the scale choice. We note that for small orifices, the Froude number has greater values, so the gravity becomes negligible in this case. On the other hand, the Reynolds number has small values, especially for ink, so the viscous effects may be important. In this paper the model includes partially viscous effects, namely those characteristic to irrotational flows. These effects show themselves via the normal viscous stress at the interface. Irrotational flow is usually a good approximation for low viscosity fluids, set in motion from rest.

We present in Figures 3 and 4 the interface temporal evolution during the DOD process, for a water drop, and an ink drop, issuing into air. For water, the orifice radius is $R = 35\mu m$, and the characteristic numbers are: $Fr = 6064$, $We = 1$ and $Re = 50.3$. For ink, the orifice radius is $R = 13\mu m$, and the characteristic numbers are: $Fr = 20125$, $We = 1$ and $Re = 2.44$.

The dimensional volume of the ejected water drop is of $77\, pl$. The equivalent radius of that drop (the radius of a sphere with the same volume) is of $26.4\mu m$. The dimensional volume of the ejected ink drop is of $5.58\, pl$, and its equivalent radius is of $11\mu m$. Thus the ejected drop size is respectively about 75%, and 85% of the orifice size, for water, and ink case, which is consistent with available DOD data.

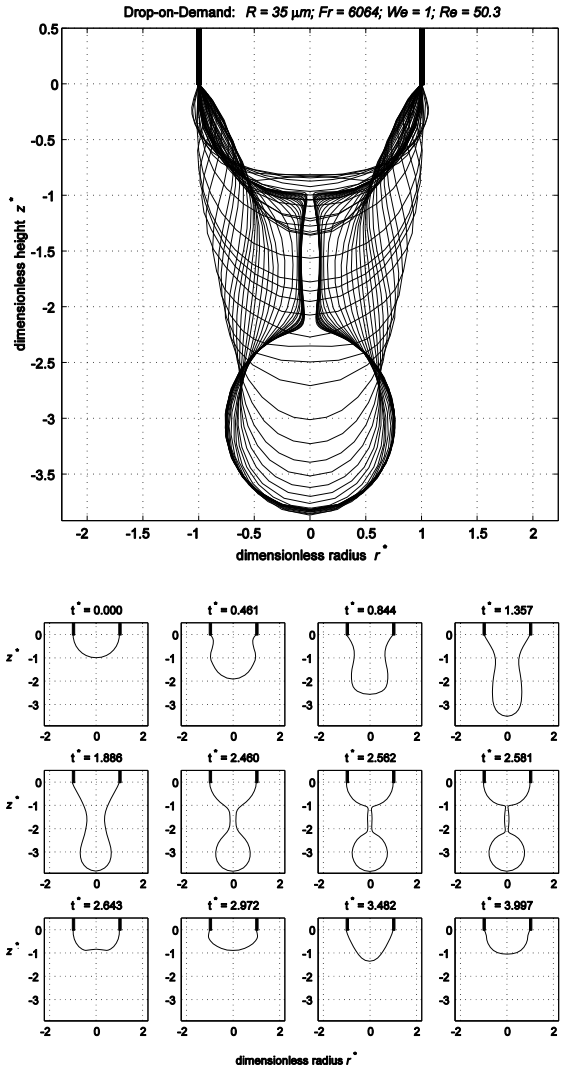

Figure 3. Superposed profiles (upper image), and some characteristic profiles at specified time t^* in separate frames (lower images), of the interface evolution, for a water drop formed by piezoelectrically driven DOD technology at an orifice of radius $R = 35\mu m$

The temporal variation of the velocity of the interface apex (i.e. the normal velocity of the node placed on the interface, on the O*z* axis), during the interface evolution, is presented in Figure 5, for the water case (upper frame), and ink case (lower frame). The instant corresponding to drop ejection is marked on the figure, for both cases. The ejection time is $t^* = 2.61$ for the water drop, and $t^* = 3.416$ for the ink drop. For water, the interface apex

oscillates during the first 20% of the time period, and also after the drop ejection instant, and recovers its initial shape at the end of the time period. Due to the viscosity, which damps inertial effects, the interface apex for ink is more stable, and after the drop ejection instant, the interface recovers quickly its initial shape, so the DOD process can continue after a shorter time period. This should help working at a higher frequency with ink.

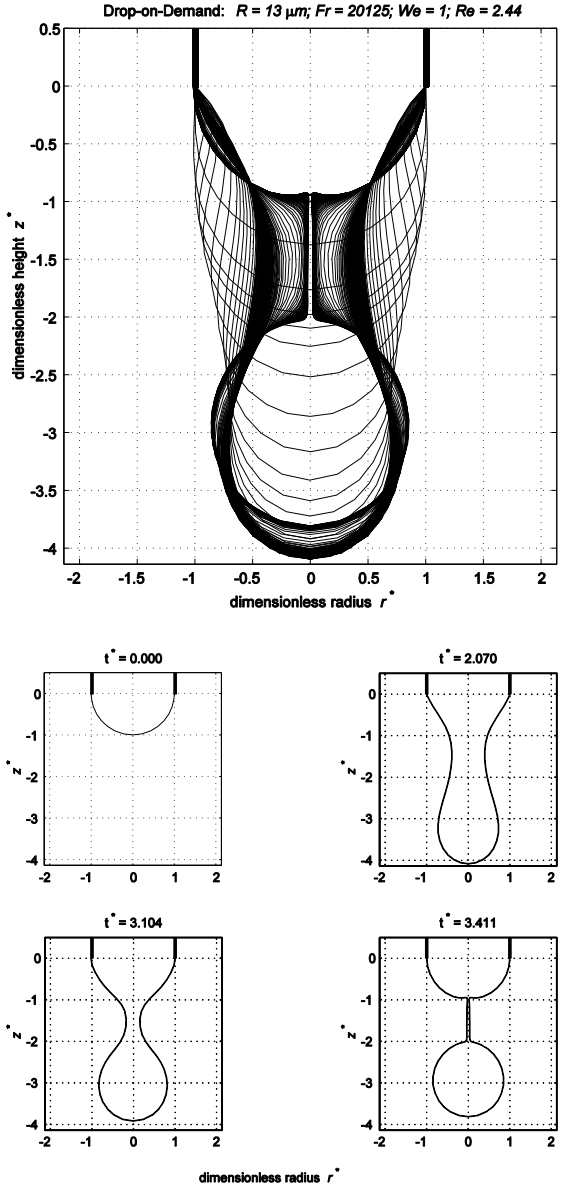

Figure 4. Superposed profiles (upper image), and some characteristic profiles at specified time t^* in separate frames (lower images), of the interface evolution, for an ink drop formed by piezoelectrically driven DOD technology at an orifice of radius $R = 13\,\mu m$

The conditions for obtaining different drop shapes immediately after ejection have been examined. We did recover the observed columnar liquid bridge joining the nascent drop to its parent body. This stage precedes necking and drop separation. In Figs 3 and 4 it is not clear whether the effective necking occurs at the upper or lower part of the column. The break-up occurs at the upper part of the column, at $z^* = -0.872$ for water, and $z^* = -0.966$ for ink case. The ejected drop shape is like the one plotted at $t^* = 2.581$ in Fig. 3 (just before the water drop detachment at $t^* = 2.61$), or like the one plotted at $t^* = 3.411$ in Fig. 4 (just before the ink drop detachment at $t^* = 3.416$).

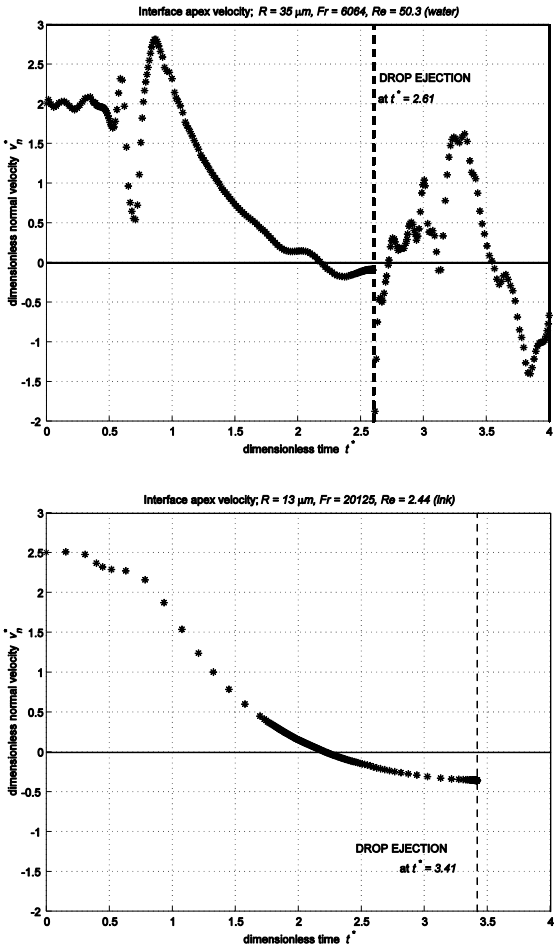

Figure 5. Temporal variation of the interface apex velocity during the DOD evolution, for the water case (upper frame), and ink (lower frame)

At the necking instant, unbalanced surface tension rapidly accelerates liquid in both liquid bodies [30]: this is the recoil stage. Waves due to separation then propagate along the column that has become a drop tail and may generate one or several satellites. This stage is difficult to be captured numerically in all the details. However some attempts have been made to describe the unique satellite formation. As the ejected ink drop from Fig.4 has a thin neck, it can be assumed that there will be a second pinching at the connection between

the long neck and the parent drop. That will lead to a satellite, which size can be estimated from the neck volume (a quasi-cylindrical shape, of 0.974 height and 0.026 mean dimensionless radius); the corresponding dimensional volume of the satellite is of $0.0045\,pl$, and equivalent radius of about $1\,\mu m$. This represents a ratio of 0.09 between the satellite radius and its parent drop radius.

With respect to industrial applications, there are desirable configurations as those leading to a simple neck pinching and drop detachment, but also undesirable configurations that must be avoided (e.g. with a wide neck). For too small values of the velocity inside the capillary nozzle, drops may not be successfully ejected (e.g. for the same *Fr* and *Re* values as in Figs. 3 and 4, for a maximum value of $v_n^* = 0.6$ for water, and $v_n^* = 2$ for ink, there is no drop ejection). In those cases, the interface grows at the beginning because of the velocity pulse, but the liquid has not sufficient inertia, and capillary effects pull back the interface to the orifice, then the drop hangs up and oscillates slowly.

Our computed results fit well the available numerical and experimental DOD data [8-12] for drops with volume of picolitres order. Encouraging agreement is obtained, but the numerical model will require added sophistication, like the evaluation of the whole viscosity effects, which would result in the introduction of the rotational part of the flow, before detailed agreement can be expected, especially for ink drops, which are much viscous than water. Moreover surfactants tend to migrate to interface when area is created during growth in order to restore the interfacial equilibrium conditions. As this process has a long time scale compared to hydrodynamic scales, they may affect the end of drop formation.

5. SUMMARY AND PERSPECTIVES

The Drop-on-Demand numerical simulation was made through a Boundary Element Method, by taking into account the capillary effects and only partially the viscous effects. In order to prevent numerical instabilities, the progression time step was obtained from a gravity-capillary waves stability criterion. The precision of the numerical code was checked through the global mechanical energy balance.

Our computed results fit well the available numerical and experimental data, for water and ink drops, with volume of picolitres order.

The present modelling can be refined in the future, by introducing the Helmoltz decomposition [31] in order to incorporate the rotational part of the velocity field, thus to evaluate the whole viscosity effects. We have to address the vorticity – stream function formulation of axisymmetric unsteady incompressible flows in conjunction with moving boundaries. The BEM leads in these cases to domain integrals that detract from the boundary only features. There are several techniques to preserve advantages of the BEM and to extend its theoretical foundations and numerical implementation to tackle this broader class of equations. One technique that we will use is based on the Greengard and Strain algorithm [32].

ACKNOWLEDGEMENTS

This work has been supported by the Programme ECO-NET from the French Ministry of Foreign Affairs, under the project “Stimulation et formation de goutte à la demande: étude expérimentale et numérique des effets non-linéaires” (2004-2005), led by professor A. Soucemarianadin from LEGI Grenoble, and by the Romanian National University Research Council (CNCSIS), under the project “DOD numerical simulation, applied in microfluidics” (2004-2005), Grant A-1405, led by S.-C. Georgescu.

REFERENCES

[1] Le, H. P., 1999, “Progress and Trends in Ink-Jet Printing Technology”, In: *Recent Progress in Ink Jet Technologies II*, ed. E. Hanson, IS&T, Springfield, pp. 1-14.

[2] Pimbley, W. T., and Lee, H. C., 1977, “Satellite Droplet Formation in a Liquid Jet”, *IBM J. Res. Develop.*, Vol. 21 (1), pp. 21-30.

[3] Hilbing, J., and Heister, S., 1996, “Droplet size control in liquid jet breakup”, *Phys. Fluids*, Vol. 8 (6), pp. 1574-1581.

[4] Lopez, B., Soucemarianadin, A., and Attané, P., 1999, “Break-up of Continuous Liquid Jets: Effect of Nozzle Geometry”, *J. Imaging Sci. Techn.*, Vol. 43 (2), pp. 145-152.

[5] Soucemarianadin, A., Pierron, P., Normandin, M., Clermont, J.R., and Attané, P., 1999, “Modeling of Liquid Jet Break-up and Drop Formation”, In: *Recent Progress in Ink Jet Technologies II*, Springfield, pp. 218-222.

[6] Chen, T., 2005, “Recent Advances in Piezoelectric Inkjet Print Head Technology”, Proc. *IS&T’s NIP21*, Baltimore, pp. 268-268.

[7] Bogy, D. B., and Talke, F. E., 1984, “Experimental and Theoretical Study of Wave Propagation Phenomena in Drop-on-Demand Ink Jet Devices”, *IBM J. Res. Develop*., Vol. 28 (3), pp. 314-321.

[8] Blumberg, A., and Semiat, R., 2002, “Velocity Measurements of Ink Drops Ejected from a Piezoelectric DOD Print Head. I Technique Presentation, II Parameters of Ejecting Signal”, *J. Imaging Sci. Techn.*, Vol.46 (2), pp. 171-189.

[9] Cittadino, J. M., Mendes, E., Soucemarianadin, A., 2005, "A Tool for Monitoring Piezoelectric Micro-Pumps", Proc. *IS&T's NIP21*, Baltimore, pp. 278-282.

[10] Fromm, J. E., 1984, "Numerical Calculation of the Fluid Dynamics of Drop-on-Demand Jets", *IBM J. Res. Develop*., Vol. 28 (3), pp. 322-333.

[11] Shield, T. W., Bogy, D. B., and Talke, F. E., 1987, "Drop Formation by DOD Ink-Jet Nozzles: A Comparison of Experiment and Numerical Simulation", *IBM J. Res. Develop.*, Vol. 31 (1), pp. 96-110.

[12] Feng, J., 2002, "A General Fluid Dynamic Analysis of Drop Ejection in Drop-on-Demand Ink Jet Devices", *J. Imaging Science and Technology*, Vol. 46 (5), pp. 398-408.

[13] Bugdayci, N., Bogy, D. B., and Talke, F. E., 1983, "Axisymmetric Motion of Radially Polarized Piezoelectric Cylinders Used in Ink Jet Printing", *IBM Journal of Research and Development*, Vol. 27 (2), pp. 171-180.

[14] Bruce, C. A., 1976, "Dependence of Ink Jet Dynamics on Fluid Characteristics", *IBM J. Res. Develop*., Vol. 20 (3), pp. 258-270.

[15] Magdassi, S., Ben-Moshe, M., Berenstein, L., and Zaban, A., 2003, "Microemulsion Based Ink-Jet Ink: Properties and Performance", *J. Imaging Sci. Techn.*, Vol. 47 (4), pp. 357-360.

[16] Koltay, P., Birkle, G., Steger, R., Kuhn, H., Mayer, M., Sandmaier, H., and Zengerle, R., 2001, "Highly Parallel and Accurate Nanoliter Dispenser for High-Throughput-Synthesis of Chemical Compounds", Proc. *IMEMS Workshop*, Singapore, pp. 1-10.

[17] Wallace, D., and Hayes, D., 2002, "Solder Jet™ - Optics Jet™ - AromaJet™ - Reagent Jet - Tooth Jet and Other Applications of Ink-Jet Printing Technology", Proc. *IS&T's NIP18*, San Diego, USA, pp. 228-235.

[18] Chen, C.-T., Chiu, C.-L., and Chen, S.-S., 2004, "Simulation and Experiment of Micro-Lens Fabrication Using Droplet Deposition Method", Proc. *IS&T's NIP20*, Salt Lake City, USA, pp. 265-268.

[19] McDonald, M., Heun, S., and Tallant, N., 2002, "Advances in Piezoelectric Deposition of Organic Electronic Materials", Proc. *IS&T's NIP18*, San Diego, pp. 433-436.

[20] Shah, V., and Hayes, D., 2002, "Trimming and Printing of Embedded Resistors Using Demand-Mode Ink-Jet Technology and Conductive Polymer", Proc. *IPC Printed Circuits Expo*, Long Beach, USA, pp. 1-5.

[21] Kuroiwa, T., Ishikawa, N., Obara, D., Vinet, F., Ang, E. S., Guelbi, A., and Soucemarianadin, A., 2003, "Dispensing of Polymeric Fluids for BIO-MEMS Applications", Proc. *IS&T's NIP19*, New Orleans, USA, pp. 884-890.

[22] Joseph, D. D., Liao, T. Y., and Hu, H. H., 1993, "Drag and moment in viscous potential flow", *Eur. J. Mech. B-Fluids*, Vol. 12 (1), pp. 97-106.

[23] Georgescu, S.-C., Achard, J.-L., and Canot, É., 2002, "Jet drops ejection in bursting gas bubble processes", *Eur. J. Mech. B-Fluids*, Vol. 21, pp. 265-280.

[24] Canot, É., Georgescu, S.-C., and Vincent, S., 2005, "Test-case No 21: Gas bubble bursting at a free surface, with jet formation (PN-PE)", In: *Validation of Advanced Computational Methods for Multiphase Flows*, eds. H. Lemonnier, D. Jamet, O. Lebaigue, Begell House Inc., New York, Chapter 19, pp.135-142.

[25] Georgescu, S.-C., 1999, "Evolution d'une bulle: Formation à partir d'un orifice et éclatement à la traversée d'une surface libre", *PhD Thesis, Institut National Polytechnique de Grenoble*.

[26] Georgescu, S.-C., Canot, É., Broboană, D., and Soucemarianadin, A., 2005, "Numerical Simulation of Drop-on-Demand Jetting Applications in Microfluidics", *EUROMECH Colloquium 472 «Microfluidics and Transfer»*, Grenoble, France, pp. 139-140.

[27] Machane, R., and Canot, É., 1997, "High-order schemes in Boundary Element Methods for transient non-linear free surface problems", *Int. J. Numer. Methods Fluids*, 24, pp. 1049-1072.

[28] Canot, É., 1999, "Stability Criteria for Capillary/Gravity Free-Surface Waves in BEM Simulations of Viscous Potential Flows", Proc. *Int. Conf. Boundary Element Techniques*, ed. M. H. Aliabadi, London, U.K., pp. 321-330.

[29] Spangler, C., Hilbing, J., and Heister, S., 1995, "Nonlinear modeling of jet atomization in the wind-induced regime", *Phys. Fluids*, Vol. 7 (5), pp. 964-971.

[30] Peregrine, D. H, Shoker, G., and Symon, A., 1990, "The bifurcation of liquid bridges", *J. Fluid. Mech.*, Vol. 212, pp. 25-39.

[31] Machane, R., Achard, J.-L., and Canot, É., 2000, "A new velocity-vorticity Boundary Integral Formulation for Navier-Stokes equations", *Int. J. Numer. Methods Fluids*, Vol. 34, pp. 47-63.

[32] Greengard, L., and Strain, J., 1990, "A fast algorithm for the evaluation of heat potentials", In: *Communications on Pure and Applied Mathematics*, XLIII, John Wiley & Sons, pp. 949-963.